

Chaotic and turbulent behavior of unstable one-dimensional nonlinear dispersive waves

David Cai^{a)} and David W. McLaughlin
*Courant Institute of Mathematical Sciences, New York University,
New York, New York 10012*

(Received 16 November 1999; accepted for publication 28 January 2000)

In this article we use one-dimensional nonlinear Schrödinger equations (NLS) to illustrate chaotic and turbulent behavior of nonlinear dispersive waves. It begins with a brief summary of properties of NLS with focusing and defocusing nonlinearities. In this summary we stress the role of the modulational instability in the formation of solitary waves and homoclinic orbits, and in the generation of temporal chaos and of spatiotemporal chaos for the nonlinear waves. Dispersive wave turbulence for a class of one-dimensional NLS equations is then described in detail—emphasizing distinctions between focusing and defocusing cases, the role of spatially localized, coherent structures, and their interaction with resonant waves in setting up the cycles of energy transfer in dispersive wave turbulence through direct and inverse cascades. In the article we underline that these simple NLS models provide precise and demanding tests for the closure theories of dispersive wave turbulence. In the conclusion we emphasize the importance of effective stochastic representations for the prediction of transport and other macroscopic behavior in such deterministic chaotic nonlinear wave systems. © 2000 American Institute of Physics. [S0022-2488(00)01606-6]

I. INTRODUCTION

The description and understanding of turbulence remains one of the most challenging open problems in classical physics. Turbulent waves are prevalent throughout nature. Examples include waves on the surface of the ocean and storms in the atmosphere. Turbulent states involve the interaction of coherent structures with a background of fluctuating waves. This stochastic background could arise from deterministic instabilities that create spatiotemporal chaos, or from externally imposed noise, or both. The goal of theories of turbulence is to predict behavior in such chaotic systems, where only certain phenomena are possible to quantify; others may be indeterminate. One task of turbulence theory is to circumscribe what is unpredictable and what is not.

Turbulent states are so complex that their description must be statistical. Constantly, statistical descriptions of turbulent waves are being proposed and developed that would play a role for nonlinear waves similar to that played by statistical physics for mechanics—namely, to provide macroscopic descriptions of observable phenomena. These theories would (i) predict wave spectra and other macroscopic observables, and (ii) provide parametrizations of small-scale behavior for large-scale numerical simulations. The validity of these theories is very difficult to assess, primarily because of mathematical and computational difficulties in the nonlinear partial differential equations (pdes) which provide the fundamental description of the waves' evolution.

Nonlinear dispersive waves in one spatial dimension are proving to be very useful tools in the design and validation of theoretical descriptions of wave turbulence. The single spatial dimension renders the waves nearly amenable to analytical description, and certainly to careful and controlled numerical simulation. In this article, we will summarize some of these developments, using a class of one-dimensional nonlinear Schrödinger equations (NLS) as examples.

^{a)}Electronic mail: cai@cims.nyu.edu

NLS equations possess two distinct types of nonlinearity: “focusing” and “defocusing,” which significantly affect the behavior of the nonlinear wave. Throughout this article, we will emphasize distinctions in behavior between the focusing and defocusing cases—for completely integrable waves, for temporally chaotic waves, for spatiotemporal chaotic waves, and for dispersive wave turbulence. In the focusing case for NLS, waves can be linearly unstable (Sec. II). When perturbed, with one unstable mode, this modulational instability can give rise to temporal chaos (Sec. III), and with two or more instabilities, it can induce spatiotemporally chaotic wave dynamics (Sec. IV) and dispersive turbulence (Secs. V and IV). NLS equations provide some of the simplest examples of the interaction of localized coherent structures with a background of stochastic waves. Properties of this interaction will be described throughout the article.

The mathematical methods used in these studies of nonlinear dispersive waves include rigorous and formal analysis of pdes, dynamical systems theory (for pdes), geometric singular perturbation theory, stochastic equations, and scientific computation.

In Sec. II, “Background,” we define a class of NLS equations with focusing and defocusing nonlinearities, and we describe the “modulational instability” in the focusing case. We also mention the “completely integrable” NLS equation, and its integration through the “inverse spectral transform.” For this integrable case, distinctions between focusing and defocusing nonlinearities are again emphasized—with the very special localized waves known as “solitons” occurring in the focusing case.

In Sec. III, representations of “homoclinic orbits” are presented for the integrable focusing case, under spatially periodic boundary conditions, and their role in the generation of temporal chaos under weakly damped and driven deterministic perturbations is discussed.

In Sec. IV, spatiotemporal chaos is defined and shown to exist for deterministic damped and driven perturbations of NLS, in the focusing case. We note in passing that there is a great deal of work on the phenomena of spatiotemporal chaos for the Ginzburg–Landau equation and for the Kuramoto–Sivashinsky equation (see a review,¹ and references therein).

In Sec. V, *dispersive wave turbulence* is summarized, within the context of a family of NLS equations. The weak turbulence theory of dispersive waves is a mathematical theory of the flow of excitations between spatial scales. It involves beautiful mathematical concepts—including resonant wave–wave interactions, normal forms for Hamiltonian systems, stochastic closures, and kinetic equations for correlation functions.

In Sec. VI, new numerical experiments on dispersive wave turbulence are described for this family of NLS equations. The dependence of the turbulent state upon focusing and defocusing nonlinearities is emphasized, as well as the interaction of coherent structures with resonant radiation in setting up the cycles of energy transfer in dispersive wave turbulence.

While dispersive wave turbulence provides a description of the intrinsic stochastic background, an *effective stochastic dynamics* will be required to provide a tool for the prediction of observable behavior. Theories that describe the interaction of coherent structures with a background of fluctuating waves (that is, with an “active heat bath”) are needed to provide an algorithm for the prediction of macroscopic transport behavior. These matters of predictability are discussed in the Conclusion.

The material in Secs. II, III, and IV on integrability, instabilities, homoclinic orbits, temporal chaos, and spatiotemporal chaos has been discussed in detail in the two surveys.^{2,3} Here we present a condensed version—emphasizing distinctions between focusing and defocusing nonlinearities, as well as consequences of the modulational instability and spatially localized coherent structures. These features in dispersive wave turbulence are highlighted in Sec. VI, which contains new material only partially announced in Ref. 4. This section, together with the Conclusion on predictability, looks toward future work.

II. BACKGROUND

The classical NLS equation in one spatial dimension is of the form

$$iq_t = q_{xx} + 2(q\bar{q})q, \quad (1)$$

with the $+(-)$ sign denoting focusing (defocusing) nonlinearity. It is a Hamiltonian system,

$$iq_t = \frac{\delta H}{\delta \bar{q}}, \tag{2}$$

with the Hamiltonian

$$H(q, \bar{q}) \equiv \int \{q_x \bar{q}_x \pm |q \bar{q}|^2\} dx. \tag{3}$$

Note that the Hamiltonian is indefinite in the focusing case. The Hamiltonian, L^2 norm, and linear momentum are constants of motion—associated to the symmetries of time, phase, and space translation, respectively. For focusing nonlinearity, the equation supports localized traveling wave solutions of the form

$$q(x, t; \lambda, v, \gamma, x_0) = \lambda \operatorname{sech}[\lambda(x - x_0 - vt)] e^{(i/4)[(v^2 - 4\lambda^2)t - 2vx + \gamma]}. \tag{4}$$

This wave is (exponentially) localized in space, and has many of the characteristics of a ‘‘particle.’’ The parameters $(\lambda, v, \gamma, x_0)$ represent its amplitude (inverse-width), velocity, phase, and spatial location, respectively. This particle-like wave travels at constant velocity v and is very stable to perturbations of both the initial data and the equation. The stability and properties of this solitary wave have been established with many numerical experiments in the physical literature, with formal asymptotics, and with rigorous pde analysis.

But the solitary waves of the one-dimensional cubic NLS equation have far more remarkable properties than merely linear stability; namely, they emerge from direct collisions with other solitary waves *completely unscathed*. Their velocities and shapes are not altered by the collision. In fact, the only consequence of the nonlinear collision is a phase shift in their relative locations. This remarkable stability under collisions makes the solitary waves of one-dimensional (1-D) cubic NLS equation behave as particles under elastic collisions. Solitary waves that satisfy this elastic collision property are called *solitons*, to emphasize the particle-like properties of these nonlinear waves.

A. Integrability of NLS

The 1-D cubic NLS equation (1) is equivalent to the following linear system:⁵⁻⁷

$$\begin{aligned} \varphi_x &= U^{(\lambda)} \varphi, \\ \varphi_t &= V^{(\lambda)} \varphi, \end{aligned} \tag{5}$$

where

$$\begin{aligned} U^{(\lambda)} &\equiv i\lambda \sigma_3 + i \begin{pmatrix} 0 & q \\ \mp \bar{q} & 0 \end{pmatrix}, \\ V^{(\lambda)} &\equiv i[2\lambda^2 + \omega^2 \pm (q\bar{q} - \omega^2)]\sigma_3 + \begin{pmatrix} 0 & 2i\lambda q + q_x \\ \mp(-2i\lambda\bar{q} + \bar{q}_x) & 0 \end{pmatrix}, \end{aligned} \tag{6}$$

and where σ_3 denotes the Pauli matrix $\sigma_3 \equiv \operatorname{diag}(1, -1)$. This equivalence follows from the integrability condition for the overdetermined linear system (5): Note that system (5) consists in two equations for only one unknown φ . As such, it is overdetermined and will possess a solution iff $\varphi_{t,x} = \varphi_{x,t}$. Explicitly calculating this condition, using system (5), shows that the integrability condition is equivalent to the NLS equation (1).

The Zakharov–Shabat linear system (5) is a ‘‘Lax pair for NLS.’’^{6,7} From it, the nonlinear Schrödinger equation (1) inherits a ‘‘hidden linearity,’’ which is the key to an explanation of the

truly remarkable properties of 1-D NLS. This discovery by Zakharov and Shabat⁷ of the Lax Pair for NLS was an extremely important step in the history of soliton theory. It showed that the earlier integration of the Korteweg-de Vries equation by Gardner, Greene, Kruskal, and Miura⁵ was not a single isolated example; rather, it was a part of a general integration procedure for certain nonlinear dispersive waves. Moreover, the NLS equation has far richer phenomena than KdV. Thus, the work of Zakharov and Shabat showed that a nonlinear equation with rich phenomena arising from instabilities could be integrated through linear spectral methods.

The primary way the ‘‘hidden linearity’’ has been used to study 1-D NLS begins from the ‘‘x flow’’ of (5):

$$\hat{L}\varphi = \lambda\varphi, \quad (7)$$

where

$$\hat{L} \equiv -i\sigma_3 \frac{d}{dx} - \begin{pmatrix} 0 & q \\ \pm \bar{q} & 0 \end{pmatrix}. \quad (8)$$

This linear ‘‘x flow’’ is viewed as a Sturm–Liouville eigenvalue problem, with eigenvalue parameter λ . The spectral and inverse spectral theory for this differential operator leads to the complete integration of the NLS equation.

For example, consider the 1-D NLS equation (1) on the whole line ($-\infty < x < +\infty$), for smooth rapidly decaying functions of x ; i.e., in Schwarz class. [Actually, in the defocusing case, $|q(x)| \rightarrow c > 0$, while in the focusing case, the limit c vanishes.] Consider the ‘‘Zakharov–Shabat’’ operator \hat{L} , Eq. (8), as an (unbounded) differential operator on $L^2(\mathbb{R})$. Denote its point spectra [eigenvalues with $L^2(\mathbb{R})$ eigenfunctions] by $\{\lambda_1, \lambda_2, \dots, \lambda_N\}$. As the coefficients $q(x, t)$ of this differential operator evolve in time t according to the 1-D NLS equation (1), one expects the eigenvalues $\lambda_j(t)$ to change with time. But they do not! A simple calculation using the Lax pair (5) shows that the eigenvalues are constant in t . These eigenvalues provide N invariants for the 1-D NLS equation (1)—where the number N , as determined by the initial data, can be very large and often exceeds three, the number of classical invariants. Thus, the 1-D NLS equation possesses some unusual invariants, in addition to the classical ones.

These additional invariants arise after considering the eigenvalues as functionals of the coefficients $q(\cdot, t)$:

$$\lambda_j(t) = \lambda_j[q(\cdot, t)].$$

This viewpoint leads one to consider the inverse problem of determining $q(\cdot, t)$ from spectral data of the differential operator \hat{L} . Clearly the finite number N of eigenvalues will be insufficient data to determine the function $\{q(x, t), \forall x \in (-\infty, +\infty)\}$, and the eigenvalues will have to be augmented with additional spectral data. But this is a well-known problem in mathematical physics known as the ‘‘inverse scattering problem’’—particularly so for the Schrödinger operator of nonrelativistic quantum mechanics, but also for the operator \hat{L} , which is a form of the Dirac operator of relativistic quantum mechanics.

This viewpoint from inverse spectral theory shows that the discrete bound state eigenvalues $\{\lambda_1, \lambda_2, \dots, \lambda_N\}$ and a continuum of reflection coefficients $\{r(\lambda), \forall \lambda \in (-\infty, \infty)\}$ are constants of motion for 1-D cubic NLS. This infinite collection of constants of motion explains the remarkable stability and elastic collision properties of solitons: First, one must understand the connection between spectral data and solitons. A formula for N solitons exists that establishes that there is a one-to-one correspondence between the solitons in the spatial profile and the bound state eigenvalues in the spectral data. The N eigenvalues correspond to N solitons, with the amplitude and speed of each fixed by the real and imaginary part of the associated eigenvalue. Moreover, a reflection coefficient $r(\lambda)$ in the spectral data of the Zakharov and Shabat operator fixes the amplitude of the λ^{th} radiative component of the nonlinear wave. The temporal behavior of the

spectral data shows that the speeds and amplitudes of the solitons are invariant in time, and are not altered by “interactions of the solitons.” And, since $|r(\lambda, t)| = |r(\lambda, 0)|$, no radiation can be generated by these interactions. In other words, the infinite number of invariants so rigidly constrain the solution that the elastic collision properties of 1-D NLS (1) result!

Such spectral considerations have led to the complete integration of the NLS equation (1), under either “whole-line” or “periodic” spatial boundary conditions—and have provided detailed explanations of the remarkable properties of solutions of this equation. Equation (1) is a *completely integrable Hamiltonian system*.

B. Modulational instability

There is an important instability for the NLS equation with *focusing nonlinearity*, known as the “modulational instability,” which is responsible for soliton formation, collapse to singular structures in finite time (in dimensions $D > 1$), unstable tori and homoclinic orbits, and temporal and spatiotemporal chaos for perturbed NLS equations. Under periodic spatial boundary conditions, specific examples of this instability are easy to describe.

Consider elementary “plane wave solutions” of the NLS equation:

$$q_c(x, t; c, \gamma) = c \exp[-i(2c^2t + \gamma)], \tag{9}$$

where (c, γ) denote two real parameters. Linearizing the NLS equation about this exact solution yields

$$q(x, t) = q_c(x, t) + \delta f(x, t) \exp[-i(2c^2t + \gamma)];$$

$$if_t = f_{xx} + 2c^2f + 2c^2\bar{f} + O(\delta);$$

$$f(x, t) = \hat{f}(k) \exp[i(kx - \omega(k)t)];$$

$$\omega^2(k) = k^2[k^2 - 4c^2].$$

From this dispersion relation $\omega(k)$, the plane wave (9) is unstable to fluctuations with wave numbers $0 < k^2 < 4c^2$; while shorter-wavelength fluctuations are neutrally stable according to linear stability theory. The “quantization condition” that ensures spatial periodicity,

$$k_j = \frac{2\pi j}{l}, \quad j = \dots, -1, 0, +1, \dots,$$

shows that the number of unstable Fourier modes scales linearly with the size l of the periodic spatial domain. This instability of the plane wave (9) to long-wavelength fluctuations is a special case of a famous instability in nonlinear dispersive wave theory, known as the “Benjamin–Feir instability” in the context of water waves⁸ and as the “modulational instability” in the context of plasma physics.⁹ This instability is only present in the case of focusing nonlinearity. Plane wave solutions of defocusing NLS are neutrally stable.

III. HOMOCLINIC ORBITS AND TEMPORAL CHAOS

Under periodic spatial boundary conditions, solutions of the integrable NLS equation reside on tori (which arise as the level sets of the constants of motion). For focusing nonlinearity, these tori can be unstable due to the modulational instability. (The level sets have a “saddle structure” in functional space.) In this setting, the spectral transform provides representations of these tori, and explicit representations of their unstable manifolds and homoclinic orbits.^{10,11} Next, we describe these representations.

Fix a periodic solution of NLS that is quasiperiodic in t , unstable, and for which the operator $\hat{L}(q)$ has a complex double eigenvalue ν of multiplicity 2. We denote two linearly independent Zakharov–Shabat eigenfunctions at (ν, q) by (ϕ^+, ϕ^-) . Thus, a general solution of the Zakharov–Shabat linear system (5) at (q, ν) is given by

$$\phi(x, t; \nu; c_+, c_-) = c_+ \phi^+ + c_- \phi^-.$$

We use ϕ to define a transformation matrix G by

$$G = G(\lambda; \nu; \phi) \equiv N \begin{pmatrix} \lambda - \nu & 0 \\ 0 & \lambda - \bar{\nu} \end{pmatrix} N^{-1}, \tag{10}$$

where

$$N \equiv \begin{bmatrix} \phi_1 & -\bar{\phi}_2 \\ \phi_2 & \bar{\phi}_1 \end{bmatrix}.$$

Then we define Q and Ψ by

$$Q(x, t) \equiv q(x, t) + 2(\nu - \bar{\nu}) \frac{\phi_1 \bar{\phi}_2}{\phi_1 \bar{\phi}_1 + \phi_2 \bar{\phi}_2} \tag{11}$$

and

$$\Psi(x, t; \lambda) \equiv G(\lambda; \nu; \phi) \psi(x, t; \lambda), \tag{12}$$

where ψ solves the Zakharov–Shabat linear system (5) at (q, λ) . Formulas (11) and (12) are the Bäcklund transformations of the potential and eigenfunctions, respectively. We^{10,11} have the following.

Theorem III.1: Define $Q(x, t)$ and $\Psi(x, t; \lambda)$ by (11) and (12). Then (i) $Q(x, t)$ is a solution of NLS, with spatial period l ; (ii) The spectrum $\sigma(\hat{L}(Q)) = \sigma(\hat{L}(q))$; (iii) $Q(x, t)$ is homoclinic to $q(x, t)$ in the sense that $Q(x, t) \rightarrow q_{\theta_{\pm}}(x, t)$, exponentially as $\exp(-\sigma_{\nu}|t|)$ as $t \rightarrow \pm\infty$. Here $q_{\theta_{\pm}}$ is a “torus translate” of q , σ_{ν} is the nonvanishing growth rate associated to the complex double point ν , and explicit formulas can be developed for the growth rate σ_{ν} and for the translation parameters θ_{\pm} ; (iv) $\Psi(x, t; \lambda)$ solves the linear system (5) at (Q, λ) .

This theorem is quite general, constructing homoclinic solutions from a wide class of starting solutions $q(x, t)$. Its proof is one of direct verification, following the sine-Gordon model.¹⁰ Periodicity in x is achieved by choosing the transformation parameter $\lambda = \nu$ to be a double point.

Several qualitative features of these homoclinic orbits should be emphasized: (i) $Q(x, t)$ is homoclinic to a torus, which itself possesses rather complicated spatial and temporal structure, and is not just a fixed point; (ii) nevertheless, the homoclinic orbit typically has still more complicated spatial structure than its “target torus.” (iii) When there are several complex double points, each with a nonvanishing growth rate, one can iterate the Bäcklund transformations to generate more complicated homoclinic manifolds. (iv) The number of complex double points with nonvanishing growth rates counts the dimension of the unstable manifold of the critical torus in that two unstable directions are coordinatized by the complex ratio c_+/c_- . Under even symmetry only one real dimension satisfies the constraint of evenness. (v) These Bäcklund formulas provide coordinates for the stable and unstable manifolds of the critical tori; thus, they provide explicit representations of the critical level sets, which consist in “whiskered tori.”¹²

The simplest examples of these homoclinic orbits begins with the spatially uniform plane wave q_c , Eq. (9), for which the entire construction can be carried out explicitly.^{11,3} Rather than repeat this simple analytical formula, we just show sample homoclinic orbits that result in Figs. 1, 2, and 3.

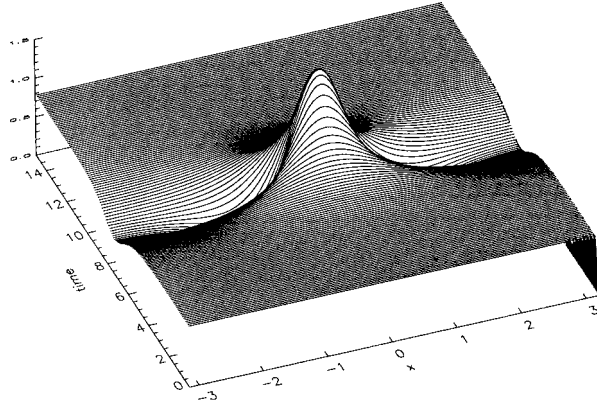


FIG. 1. Homoclinic orbit associated with one instability: Center location. Plotted is $|q(x,t)|$.

In this example the target is always the plane wave; hence, it is always a circle of dimension one, and in this example we are constructing whiskered circles. On the other hand, in this example the dimension of the whiskers need not be one, but is determined by the number of purely imaginary double eigenvalues, which in turn is controlled by the amplitude c of the plane wave target and by the spatial period. (When there are several complex double points, the Bäcklund transformations must be iterated to produce complete representations of the unstable manifold.)

Thus, Bäcklund transformations give global representations of the critical level sets. The level sets in the neighborhood of these of critical ones have fascinating topological structure.^{13,11} The plane wave example under even symmetry and with only one instability provides the simplest case. Here, the dimension of the unstable manifold of the plane wave circle is 2—the dimension of each homoclinic orbit plus the dimension of the target circle $q=S$. In addition, NLS also possesses a four-dimensional invariant manifold that contains the unstable manifold $W^u(q=S)$. This 4-D manifold can be viewed as the result of “shutting-off” all degrees of freedom except for the spatial mean and the “first radiation mode.” In this four-dimensional space, the level sets topologically form a trouser diagram shown in Fig. 4. Note in particular the symmetric pair of homoclinic orbits and their relationship to the two legs, one of which represents a (periodic) soliton located at the center of the periodic domain at $x=0$, and the other a soliton located one-half period away at $x=l/2$. When all other radiation degrees of freedom are excited, each forms a small disk (a center for each additional radiation degree of freedom), and the full phase space can be represented topologically (locally, near the trouser) as the product of the trouser with a countable number of disks. More complex examples are described in Ref. 11.

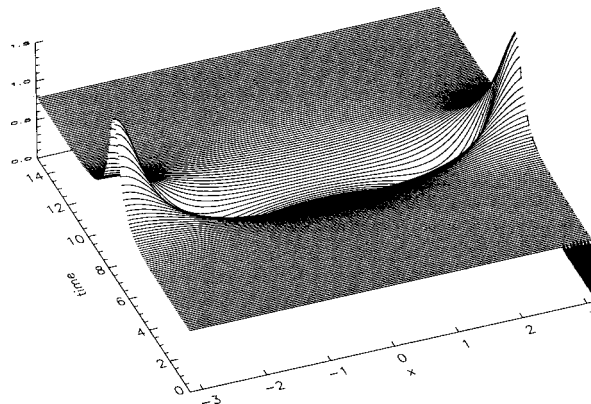


FIG. 2. Homoclinic orbit associated with one instability: Edge location (cf. Fig. 1).

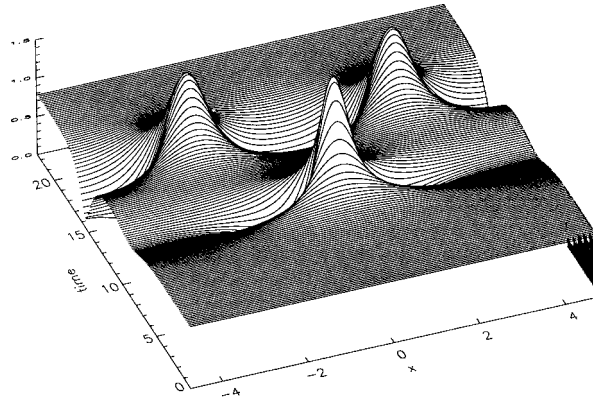


FIG. 3. Homoclinic orbit associated with two instabilities (cf. Fig. 1).

A. Temporal chaos

The existence of instabilities and their associated homoclinic orbits for the integrable NLS equation indicate that external perturbations could induce chaotic responses in perturbed deterministic NLS equations. Moreover, the trouser topology nearby critical level sets, together with the correlation of the two legs of the trouser with two distinct spatial locations for a soliton (“center” and “edge” of the periodic domain), indicates that chaotic behavior under deterministic perturbations might involve a “random jumping” of a solitary wave between these two spatial locations. Our numerical experiments^{14,2} show that these expectations are realized, and that these temporally chaotic states are relatively easy to observe.

In Refs. 14 and 2, we considered a damped-driven perturbation of the NLS equation in the form

$$iq_t + q_{xx} + 2|q|^2q = -i\alpha q + \Gamma e^{i(\omega t + \gamma)}, \tag{13}$$

with periodic boundary conditions, $q(x+l) = q(x)$, where l is the system length, and ω and γ are the driving frequency and phase, respectively. The damping coefficient α and the driving strength Γ are small. The initial condition is a periodic extension of the single soliton waveform,

$$q(x,0) = \eta \operatorname{sech}(\eta x). \tag{14}$$

These numerical experiments are described in detail in the survey,² including (i) the numerical algorithms and their validation, which is essential when studying long-time temporal integrations of chaotic behavior of unstable orbits; (ii) the collection of chaotic diagnostics with which we post-processed the numerical data; and (iii) a detailed discussion of our numerical observations. Here we only give a brief description of typical observations, for the simplest case where temporal chaos was observed.

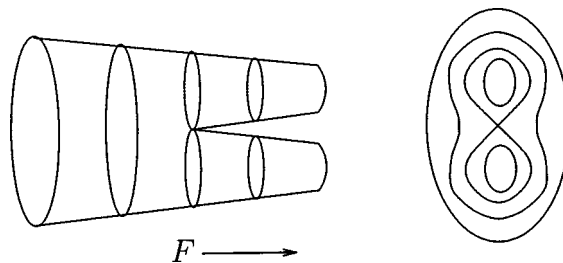


FIG. 4. Trouser diagram: One of the legs corresponds to the center location (Fig. 1) and the other to the edge (Fig. 2). The right figure is the “end view” of the trouser along the direction of the arrow. F indexes the level sets.

We organized our numerical studies into *bifurcation experiments* in which all parameters were fixed, except for the amplitude of the driving force Γ , which was increased from experiment to experiment as a ‘‘bifurcation parameter.’’ Sample results are pictured in Fig. 5. While the details of the bifurcation sequence are somewhat involved,² the general pattern may be summarized as follows. As Γ increases, the long-time behavior of the wave undergoes the following sequence of changes: (i) spatially flat, time independent; (ii) ‘‘sech-like’’ in space, time independent; (iii) sech-like in space, but time periodic; (iv) sech-like in space with a background, quasiperiodic in time; (v) chaotic in time, with the sech-like excitation jumping from the center to the edge of the periodic spatial domain, which should be compared with the homoclinic orbits in Figs. 1 and 2. Standard chaotic diagnostics² were used to identify chaotic behavior—including Poincaré sections, power spectra, Lyapunov exponents, and information dimension. Figure 5 shows four sample ‘‘cross sections’’—for time-independent, periodic, quasiperiodic, and chaotic temporal behavior.

This experiment is the simplest that we have found that has chaotic behavior, and it is very important for our theoretical studies. In it, the chaotic state contains only one spatially localized coherent structure. At times this solitary wave is located at the center, and at other times at the edges of the periodic spatial domain. These two locations are the only two allowed under even boundary conditions. We believe that one source of the chaotic behavior is an irregular (random?) jumping of the solitary wave between center and edge locations (see Fig. 6). This center–edge jumping of the solitary wave through homoclinic transitions forms the basis for the simplest description and model of chaotic behavior in NLS pdes.

B. Persistent homoclinic orbits

The first step toward analytical descriptions of such chaotic behavior is to assess the persistence of homoclinic orbits. These can provide a ‘‘skeleton’’ for chaotic trajectories. That is, persistent stable and unstable manifolds, and their intersections provide a framework with which chaotic behavior can be described. Procedures for this description are well known for finite-dimensional dynamical systems,^{15,16} and have recently been developed for the NLS pde.¹⁷ See also Refs. 18 and 3 for rather detailed overviews of these mathematical arguments.

Here we merely state the persistence theorem:¹⁷ Consider a perturbed NLS equation of the form

$$iq_t = q_{xx} + 2[q\bar{q} - \omega^2]q + i\epsilon[\hat{D}q - 1], \tag{15}$$

where the constant $\omega \in (\frac{1}{2}, 1)$, ϵ is a small positive constant, and \hat{D} is a *bounded* negative definite linear operator on the Sobolev space $H^1_{e,p}$ of even, 2π periodic functions. Specific examples of the dissipation operator \hat{D} include the discrete Laplacian and a ‘‘smoothed Laplacian’’ given by

$$\hat{D}q = -\alpha q - \beta \hat{B}q, \tag{16}$$

where the operator \hat{B} has symbol given by

$$b(k) = \begin{cases} k^2, & k < \kappa, \\ 0, & k \geq \kappa. \end{cases}$$

Extending Melnikov analysis and geometric singular perturbation theory to a pde setting, we¹⁷ establish the following.

Theorem III.2: *The perturbed NLS equation (15) possesses a symmetric pair of orbits that are homoclinic to a saddle fixed point Q, provided the parameters lie on a codimension 1 set in parameter space, which is approximately described by*

$$\alpha = E(\omega)\beta.$$

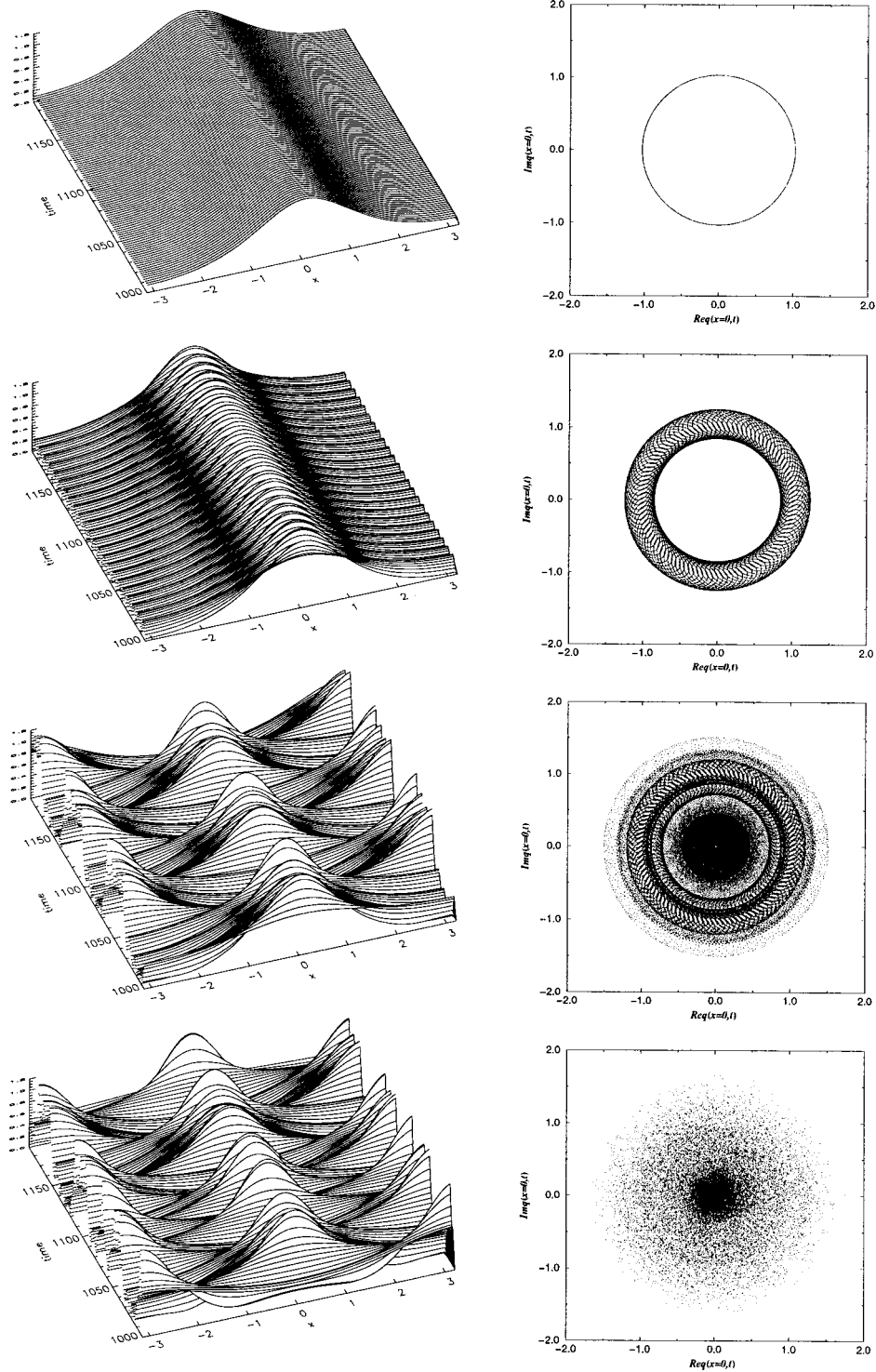


FIG. 5. Perturbed solitonic dynamics. From top to bottom: (1) locked state, (2) periodic state, (3) quasiperiodic state, and (4) temporal chaotic state (which should be contrasted with homoclinic orbits in Figs. 1 and 2). Plotted here are $|q(x,t)|$. The right panels are the corresponding surface cross sections $\{\text{Re } q(0,t), \text{Im } q(0,t), \forall t\}$. Note that for the case of the quasiperiodic and chaotic dynamics shown here, the values of the driving Γ differ only by 0.4%.

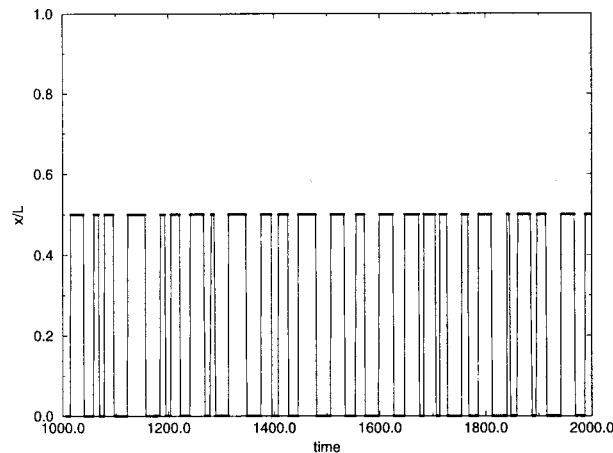


FIG. 6. Center–edge jumps of the soliton. The dark line segments are the temporal traces of the maximum of $|q(x,t)|$.

Formulas exist that describe, approximately for small ϵ , the characteristic properties of these homoclinic orbits such as the constant $E(\omega)$ and a “take-off” angle.

These two homoclinic orbits differ by the location of a transient spatial structure—a solitary wave which is located either at the center ($x=0$) or the edge ($x=\pi$) of the periodic box. As such, this theorem provides a key step toward the exciting possibility of horseshoes¹⁹ and chaotic symbol dynamics¹⁶ for the pde—with the jumping of the solitary wave between the two spatial locations as “random as a coin toss.” Recently, Li²⁰ has made a further step toward such pde behavior by establishing a symbol dynamics for an infinite dimensional geometric model of perturbed NLS.

Recent extensions and related work about temporal chaos for NLS pdes include the following:

- (1) The removal of the assumption of bounded perturbations, so that the theorem now applies to diffusion.²¹
- (2) The existence of very long (but finite) complex transients, which are more robust and easier to observe than symbol dynamics.^{22,23}
- (3) The lack of persistence of NLS homoclinic orbits under complex Ginzburg Landau perturbations.²⁴
- (4) The behavior under conservative perturbations.^{25–28}
- (5) The removal of the constraint of even symmetry.²⁷
- (6) The realization of chaotic dynamics in wave tanks.²⁹

IV. SPATIOTEMPORAL CHAOS—EXISTENCE

The *temporal chaos* just discussed consists of spatially coherent localized waves that dance chaotically in time. As Fig. 5 shows, these waves are very regular in space. Their time series at location x , $\{q(x,t), \forall t\}$, appears to be statistically well correlated to the time series at location $y \neq x$, $\{q(y,t), \forall t\}$. On the other hand, waves of *dispersive turbulence* should behave chaotically in both space and time. At least the time series $\{q(x,t), \forall t\}$ and $\{q(y,t), \forall t\}$ should become statistically independent as the distance from x to y increases.

Recall that the numerical experiment described in Sec. III was for small spatial domains, with only one instability and only one solitary wave. Intuitively, spatial decorrelation might be achieved by increasing the size l of the spatial domain (because the number of instabilities, and thus, the number of spatially localized states within the spatial domain, increases with domain size l). Spatial decorrelation is indeed seen in our numerical experiments for the damped-driven NLS (13). An example with only one instability is shown in Fig. 7, while one with two instabilities in

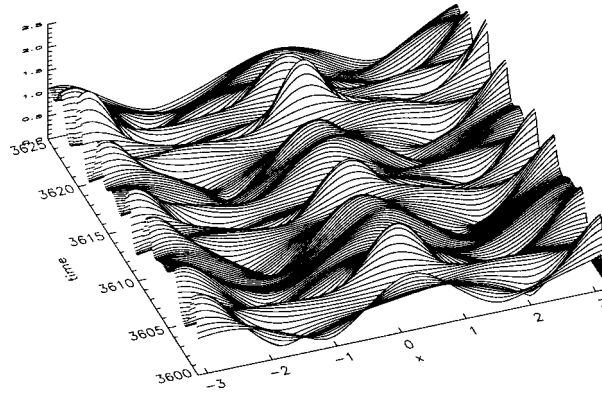


FIG. 7. Temporal chaos in the presence of one linearly unstable mode, $l=6.4$; the evolution of system (13) with $\alpha=0.004$, $\Gamma=0.144$, $\omega=1$. The initial condition $q=A+\epsilon \exp(i2\pi x/l)$, $A=0.8$, $\epsilon=2\times 10^{-5}$. Plotted here is $|q(x,t)|$.

Fig. 8. Clearly, the two figures display drastically different spatial patterns. It is instructive to compare Fig. 7 with the homoclinic orbits shown in Figs. 1 and 2 and to compare Fig. 8 with the homoclinic orbit shown in Fig. 3.

A natural question arises: Given a temporally chaotic solution of Eq. (13), how large a spatial domain, or how many instabilities, is required for effective decorrelation in space? Before investigating such questions further, we need first to formulate a precise definition of the concept of spatiotemporal chaos.

A. Definition of spatiotemporal chaos

There have been many definitions proposed to capture the essence of spatiotemporal chaos.¹ We prefer a “working definition” that includes two points: (i) A temporally chaotic wave $q(x,t)$, (ii) for which the time series $\{q(x,t), \forall t\}$ and $\{q(y,t), \forall t\}$ become statistically independent as the distance from x to y increases.

For a definition, we must make precise the meanings of “temporal chaos” and “statistical independence.” For *temporal chaos* we will accept any common definition, such as a bounded attractor with positive Lyapunov exponents.

Statistical independence is often estimated through the decay of the two-point correlation function:

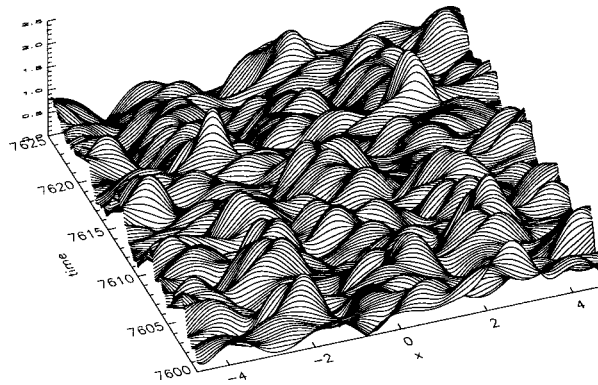


FIG. 8. Spatiotemporal chaos in the presence of two linearly unstable modes, $l=9.6$, for system (13). (For parameters see Fig. 7.)

$$C(x-y) \equiv \lim_{T \rightarrow \infty} \frac{1}{T} \int_0^T [(q(x,t) - \langle q \rangle)(\bar{q}(y,t) - \langle \bar{q} \rangle)] dt, \tag{17}$$

where $\langle \cdot \rangle$ denotes the temporal mean, and where we have assumed translational invariance of the system. However, the vanishing of the two-point correlation function is only a necessary condition for statistical independence; thus, we prefer to base the definition upon *mutual information*—whose vanishing is a necessary and sufficient condition for statistical independence.

For two stochastic variables U and V , with probability density functions $p(u)$ and $p(v)$, respectively, and with joint probability density function $p(u,v)$, the mutual information between these two variables U and V is defined as³⁰

$$\mathcal{I}(U,V) = \int du dv p(u,v) \log \frac{p(u,v)}{p(u)p(v)}. \tag{18}$$

In this application of spatiotemporal chaos, the probability distributions will be generated by the chaotic time series:

$$p_x(q): \{q(x,t), \forall t\},$$

$$p_y(q): \{q(y,t), \forall t\},$$

$$p_{x,y}(q,r): \{[q(x,t), r(y,t)], \forall t\},$$

where $r(y,t) = q(y,t)$. Intuitively, $p_x(q) dq$ is the fraction of time that $q(x, \cdot) \in (q, q + dq)$, etc. Thus, we define the mutual information between points x and y by

$$\mathcal{I}(x,y) = \int du dv p_{x,y}(u,v) \log \frac{p_{x,y}(u,v)}{p_x(u)p_y(v)}. \tag{19}$$

In terms of this mutual information between spatial points, we arrive at our working definition as follows.

Working definition: A wave $q(x,t)$ is *spatiotemporal chaotic* if (1) $q(x,t)$ is a temporally chaotic orbit (for example, as characterized by bounded, not asymptotically periodic, orbits with positive Lyapunov exponents); (2) whose mutual information between two spatial points $\mathcal{I}(x,y)$ decays exponentially in space as $|x-y| \rightarrow \infty$.

B. Numerical measurements of spatiotemporal chaos for NLS waves

Now we return to chaotic NLS waves (13) and establish by numerical experiments the existence of spatiotemporal chaos.^{31,32} First, we calculate numerically the spatial correlation function $C(x)$ [Eq. (17)].

Figure 9 shows the dependence of the correlation function $C(x)$ on the system length. For $L = 6.4$, which corresponds to the one linearly unstable mode, the whole system is correlated. This is intuitively consistent with the observations of Fig. 7, since, for most times of the evolution, only one solitary wave is present in the periodic spatial domain. When the system size is increased so that larger numbers of solitary waves are present, Fig. 9 shows that the correlation function rapidly vanishes. Therefore, the system becomes increasingly decorrelated, indicating an onset of spatiotemporal chaos. As shown in the inset of Fig. 9, the correlation at the half-system length as a function of L displays a clear transition around the value $L_{th} = 2\pi/A$, above which the second linearly unstable mode enters (note that A is the amplitude of the plane wave; see Fig. 7).

Mutual information can be used to make these results more precise. Figure 10 summarizes the mutual information as a function of the distance x between any two points in space for both one and two linearly unstable modes, which corresponds to the cases in Figs. 7 and 8, respectively. For one linearly unstable mode the mutual information remains nonzero across the system, signifying

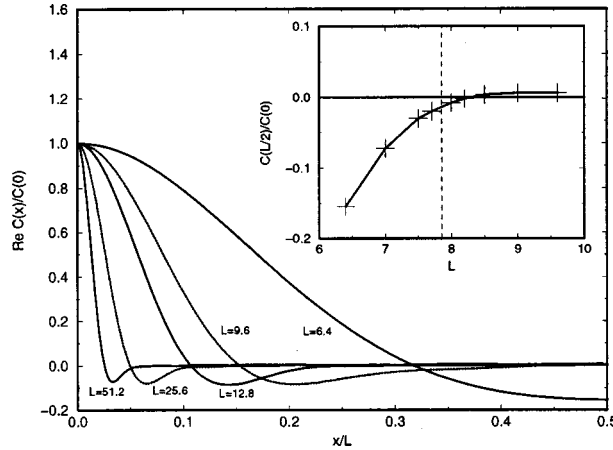


FIG. 9. Dependence of the correlation $C(x)$ on the system size L . Inset: Transition of $C(L/2)$ around $L_{th} = 2\pi/A$ (dashed line). For $L = 6.4, 9.6$, see Figs. 7 and 8.

no sufficient loss of information over the whole system, while it vanishes rapidly for the two linearly unstable mode case. It can be further determined that this decay is *exponential* as shown in the inset of Fig. 10; that is,

$$\mathcal{I}(x) \rightarrow \exp\left(-\frac{x}{\xi}\right), \quad \text{for large } x, \tag{20}$$

with a decay length $\xi \sim 0.30$. As solitons are phase locked to the external driver, i.e., $\Omega = \omega$, we anticipate that the driving frequency ω controls this decay length, i.e., the soliton's frequency Ω determines its spatial width, and hence should determine its coherence length in space.

These results establish that spatiotemporal chaos exists for NLS waves, with the transition from temporal chaos to spatiotemporal chaos occurring at the system size at which a second instability arises, provided the constraint of even symmetry is relaxed. Only *two* instabilities seem to be required—a somewhat unexpected result, as the prevalent belief in the physical literature requires very large systems with many unstable modes.^{1,33–35} (See, however, the recent work.³⁶)

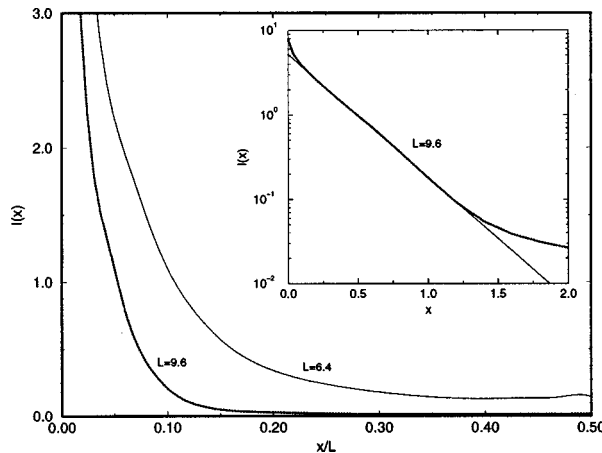


FIG. 10. Mutual information $\mathcal{I}(x)$. Fine line: one linearly unstable mode; Dotted line: two linearly unstable modes as also shown in the inset on the linear-log scale (the straight line is a fit to an exponential form).

C. Descriptions of the spatiotemporal chaotic state

Given the existence of a spatiotemporal chaotic state, one seeks ways to describe and understand it. Clearly such states are so complex that statistical descriptions will be required. Several possibilities exist, including (i) equilibrium statistical mechanics, (ii) closure theories of dispersive wave turbulence, and (iii) effective stochastic dynamics of coherent states in interaction with a background of fluctuating waves. Next, we describe this background with the methods from dispersive wave turbulence.

V. DISPERSIVE WAVE TURBULENCE

A spatiotemporal chaotic collection of waves is so complex that it must be described statistically. Ensembles of chaotic waves form a stochastic state or an “active heat bath” for which wave spectra, instead of individual wave trajectories, are natural observables. In this stochastic state, the fundamental excitations consist in resonant wave–wave interactions, which are described statistically by the theory of dispersive wave turbulence.

Dispersive wave turbulence is a theory of the flow of wave excitations between spatial scales, or fluxes, in k space. It assumes that the active stochastic state is created as a state of “statistically steady flow in k space” as follows: Excitations are being injected into the system at one spatial scale (say a long spatial scale) by an external forcing, and removed by dissipation that is restricted to a second spatial scale (say a short scale). Resonant wave–wave interactions transport the excitations, setting up a steady flow from the injection to the dissipation regions of k space. At the intermediate scales (the “inertial” or “Kolmogorov” scales), there is no forcing or damping, and the waves satisfy a conservative Hamiltonian system. These waves reside in a statistical state of steady flow in k space and their wave spectra are believed to be universal, i.e., independent of the details of forcing and dissipation.

Dispersive wave turbulence seeks equations that govern the temporal evolution of the two-point correlation functions $n(k,t)$,

$$n(k,t) \equiv \langle a(k,t)\bar{a}(k,t) \rangle,$$

where $a(k,t)$ denotes the spatial Fourier transform of the wave profile $q(x,t)$, and $\langle \cdot \rangle$ denotes an average—either an ensemble average with respect to initial conditions, a local time average, or both. In principle, averaging does not lead to “closed” evolution equations for $n(k,t)$. That is, the evolution of the two-point functions $n(k,t)$ depends upon four-point functions; those for the four-point functions depend upon six-point functions, resulting in an infinite hierarchy of equations for correlation functions. *Ad-hoc* closures have been developed through approximations that rely upon weak nonlinearity and/or Gaussian random phase assumptions. It is difficult to assess the accuracy and validity of these closure schemes, primarily because of mathematical and computational difficulties in the nonlinear pdes that provide the fundamental description of the waves.

Resonant radiation waves are the fundamental excitations that comprise the active stochastic background. However, in nonlinear wave systems, localized coherent structures often coexist with radiation. With focusing nonlinearities these localized coherent structures typically are present, and it is unnatural to restrict to nonlinearities so weak that the wave system is solely comprised of radiation. When both classes of excitations are present, it is a major theoretical challenge to obtain and validate a description of the rich structure of dispersive wave turbulence.

Here, we attempt to illustrate the richness of dispersive wave turbulence by itself, and in the presence of coherent structures, by using a class of one-dimensional nonlinear wave equations that was introduced in Ref. 37. The model is constructed such that the validity of theories of dispersive wave turbulence can be precisely checked numerically. This model permits an explicit definition of each of the concepts just described. It has both focusing and defocusing nonlinearities, and in the focusing case, has both types of excitations (localized coherent structures and resonant radiation). With this model, one obtains a very precise and detailed description of dispersive wave turbulence.

A. Background about weak turbulence

If there is only one type of wave present in a nonlinear medium, one can describe the wave in the absence of dissipation by a complex amplitude a_k satisfying the Hamiltonian system,

$$i \frac{\partial a_k}{\partial t} = \frac{\delta H}{\delta \bar{a}_k}. \tag{21}$$

We consider Hamiltonians of the form

$$H = H_0 + H_{\text{int}}, \tag{22}$$

where

$$H_0 = \int \omega(k) a_k \bar{a}_k dk$$

is the Hamiltonian of the linearized problem, $\omega(k)$ denotes its dispersion relation, and H_{int} is a perturbation describing the interaction among those degrees of freedom represented, in k space, by a_k . Generally, H_{int} can be expressed in terms of power series in a_k and \bar{a}_k .

The dispersion relation $\omega(k)$ affects the nature of wave interactions and their resulting turbulence properties. For example, if

$$\begin{aligned} \omega(k) &= \omega(k_1) + \omega(k_2), \\ k &= k_1 + k_2, \end{aligned} \tag{23}$$

holds for some k , the wave coupling leads to the resonant interaction of waves a_{k_1} and a_{k_2} with $a_{k_1+k_2}$. This situation is called *three-wave resonance*. If (i) Eq. (23) does not have solutions, and if (ii)

$$\begin{aligned} \omega(k_1) + \omega(k_2) &= \omega(k_3) + \omega(k_4), \\ k_1 + k_2 &= k_3 + k_4, \end{aligned} \tag{24}$$

has nontrivial ($k_3 \neq k_1, k_2$) solutions, then four-wave resonances are responsible for the main energy transfer between weakly nonlinear dispersive waves. It can be easily shown that, under the above two conditions, a normal form near-identity transformation will place the Hamiltonian (22) in the form

$$H = \int \omega(k) a_k \bar{a}_k dk + \int S_{kk_1k_2k_3} \bar{a}_k \bar{a}_{k_1} a_{k_2} a_{k_3} \delta(\Delta_4) dk dk_1 dk_2 dk_3, \tag{25}$$

where $\Delta_4 \equiv k + k_1 - k_2 - k_3$. This is the canonical form of a Hamiltonian system with four-wave resonances. Clearly in this case, the ‘‘particle’’ number,

$$N = \int n_k dk = \int n_\omega d\omega, \tag{26}$$

is conserved and where $n_k \equiv |a_k|^2$ and $n_\omega \equiv n_k dk/d\omega$. In addition, the linear energy can be written as

$$H_0 = \int \omega_k n_k dk = \int \omega n_\omega d\omega. \tag{27}$$

B. The direct and inverse cascades

These two quantities (26) and (27) have a direct implication on the flux of energy and wave ‘‘particle’’ number under four-wave resonances with *local* interaction kernels, when the system is forced at some wave numbers and damped at others. This implication can be easily seen from global balances of ‘‘particles’’ and energy. Assuming local interaction, we consider an idealized situation in which N particles are being created per unit time at frequency ω , and N_- and N_+ particles are being removed at frequencies ω_- and ω_+ . In a steady state, conservation of particles and (linear) energy leads to

$$N = N_- + N_+,$$

$$\omega N = \omega_- N_- + \omega_+ N_+.$$

Solving for N_- and N_+ , we have

$$N_- = \frac{N(\omega_+ - \omega)}{\omega_+ - \omega_-}, \tag{28}$$

$$N_+ = \frac{N(\omega - \omega_-)}{\omega_+ - \omega_-}. \tag{29}$$

Since $N_-, N_+ > 0$, ω has to lie between ω_- and ω_+ . Without loss of generality, we choose $\omega_- < \omega < \omega_+$. As neither N_-, N_+ nor $\omega_- N_-, \omega_+ N_+$ vanish, there are fluxes of particles and energy in both directions from ω . If ω_- is near zero, there will be almost no energy removal at the low frequencies, and the energy will flow upward from ω to ω_+ , resulting in an upward (direct) cascade of energy from the low frequencies to the high ones. If ω_+ is very large, Eq. (29) shows that the number of particles removed at ω_+ will be very small, and the particles have to flow from ω to ω_- , creating a downward (inverse) cascade of particles. As a consequence, if the dissipation takes place only at frequencies near zero and at very high values, there is an ‘‘inertial’’ range in which the energy flows upward from its source to the sink at the high frequencies, while the particles flow downward from their source to the sink at the low frequencies. As we will see below, these cascades provide an intuitive physical basis for understanding the steady flow solutions in weak-turbulence theories. However, note that nonlinearities often give rise to nonlocal interactions. Because of nonlocality, injection of energy at a particular frequency can create particles over a wide range of frequencies extremely rapidly compared with the wave-wave resonance time scale; similarly, dissipation at a particular scale can remove particles simultaneously over a range of scales. Our numerical study seems to indicate that interactions in k space are more nonlocal in many situations than usually believed.

C. A simple model problem

Consider the class of one-dimensional waves introduced in Ref. 37:

$$i q_t = |\partial_x|^\alpha q \pm |\partial_x|^{-\sigma} \left(|\partial_x|^{-\sigma} q \right)^2 |\partial_x|^{-\sigma} q, \tag{30}$$

or equivalently in ‘‘ k space,’’

$$i \dot{a}_k = \omega(k) a_k \pm \int \frac{a_{k_1} a_{k_2} \bar{a}_{k_3}}{|k_1 k_2 k_3 k|^\sigma} \delta(k_1 + k_2 - k_3 - k) dk_1 dk_2 dk_3, \tag{31}$$

where the $-(+)$ sign labels focusing (defocusing) nonlinearities. This model depends upon two real parameters, $\alpha > 0$ and σ . The parameter σ is introduced to control the nonlinearity. The parameter α controls the dispersion relation

$$\omega(k) = |k|^\alpha,$$

which, for $\alpha < 1$, has resonant quartets in this one-dimensional model.

Note that, for $\alpha \geq 1$, resonance conditions (24) have only trivial ($k_1 = k_3$ or $k_1 = k_4$) solutions. Obviously, $\alpha = 2$ and $\sigma = 0$ constitute the usual NLS equation, which has no nontrivial four-wave resonances in one dimension. We use $\alpha < 1$, and usually $\alpha = \frac{1}{2}$.

Weak turbulence theory is a statistical description of weakly nonlinear dispersive waves in terms of a closed, kinetic equation for certain two-point spectral functions. Starting with Eq. (31) in k space, one obtains

$$n_t(k, t) = \pm \int \frac{2 \operatorname{Im}(a_{k_1} a_{k_2} \bar{a}_{k_3} \bar{a}_k)}{|k_1 k_2 k_3 k|^\sigma} \delta(k_1 + k_2 - k_3 - k) dk_1 dk_2 dk_3, \tag{32}$$

for the two-point function $n(k, t) = \langle a_k(t) \bar{a}_k(t) \rangle$. Under a Gaussian random phase approximation, and the assumption that

$$\frac{\partial}{\partial t} \langle a_{k_1} a_{k_2} \bar{a}_{k_3} \bar{a}_k \rangle \approx 0,$$

justified by an asymptotics of multiscale times, one obtains the *closure condition*,

$$\operatorname{Im} \langle a_{k_1} a_{k_2} \bar{a}_{k_3} \bar{a}_k \rangle \approx \pm 2\pi \delta(\omega_1 + \omega_2 - \omega_3 - \omega) \frac{n_2 n_3 n_k + n_1 n_3 n_k - n_1 n_2 n_k - n_1 n_2 n_3}{|k_1 k_2 k_3 k|^\sigma}.$$

Using this condition, one can close Eq. (32) to arrive at

$$n_t = 4\pi \int \frac{n_1 n_2 n_3 n_k}{|k_1 k_2 k_3 k|^{2\sigma}} \left(\frac{1}{n_k} + \frac{1}{n_3} - \frac{1}{n_2} - \frac{1}{n_1} \right) \delta(\omega_1 + \omega_2 - \omega_3 - \omega) \delta(k_1 + k_2 - k_3 - k) dk_1 dk_2 dk_3, \tag{33}$$

which is the weak-turbulence kinetic equation for $n(k, t)$. It is important to note that both the *defocusing* and the *focusing* nonlinearity lead to the same kinetic equation (33). Weak turbulence does not discriminate between modulationally stable and unstable waves.

D. The wave spectra

The angular averaged kinetic equation (33)³⁷ possesses time independent (stable) solutions of the weak turbulence that describe steady-state spectra:

$$n(k) = c, \quad \text{equipartition of particle number;} \tag{34}$$

$$n(k) = \frac{c}{\omega(k)}, \quad \text{equipartition of energy;} \tag{35}$$

$$n(k) = c |k|^{8\sigma/3-1}, \quad \text{direct cascade;} \tag{36}$$

$$n(k) = c |k|^{8\sigma/3-1+(\alpha/3)}, \quad \text{inverse cascade.} \tag{37}$$

The first two ‘‘equilibrium spectra’’ can immediately be shown to satisfy (33). In fact, each is a special case of the general solution

$$n(k) = \frac{c}{\omega(k) + \mu},$$

where the constant μ denotes the “chemical potential.” The interpretation of these first two steady states as “equipartition of particles” and “equipartition of energy” comes from the invariant (26) and (27).

The other two spectra of the “direct” and “inverse” cascades were obtained by Zakharov³⁸ as special solutions of the kinetic equation. His beautiful argument uses a conformal transformation, and is motivated and described in Ref. 37 for model (30).

In the numerical experiments reported in Refs. 37 and 4, another spectrum was also observed. For Eq. (30) at $\alpha = \frac{1}{2}$, this spectrum is

$$n(k) = c|k|^{2\sigma - 5/4}, \quad \text{MMT.} \tag{38}$$

As shown in Ref. 37, the MMT spectrum is not a solution of the weak-turbulence equations (33). Rather, it satisfies an alternative closure (referred to as the MMT closure), which was heuristically proposed in Ref. 37.

VI. NUMERICAL RESULTS ON DISPERSIVE WAVE TURBULENCE

We simulate the full dynamics of system (30) using a pseudospectral method in combination with an integrating factor method. (For details, see Ref. 37). For the time dynamics, we use a fourth-order adaptive step size Runge–Kutta integrator. For most runs, the total number of modes is 2^{13} , and the system size $L \sim 400$.

In the following, we will describe some results of our numerical experiments. We will use the convention that the unit for the wave number k is $2\pi/L$: thus k is labeled by integers.

A. Four spectra

We begin in a *freely decaying* setting, in which both the direct and inverse weak-turbulence (WT) cascades are observed. These specific studies are all initialized from the same identical state (for both defocusing and focusing nonlinearities and for various σ 's and α 's), which is constructed as follows: First, a sufficiently stirred state is created from the evolution of smooth initial data under a random forcing at long wavelengths. Then, to study freely decaying turbulence, we use this state as initial data, with the force set at 0 and with damping of the form $-i\Gamma_j a_k$, $j=1,2$, with Γ_1 on large spatial scales $|k| \sim 1$, Γ_2 on small spatial scales $|k| > K_d$ ($K_d = 2600$ for most experiments) and no damping in between. When $\Gamma_1 \ll \Gamma_2$, the state gradually relaxes to the *direct* WT cascade.

As shown in Fig. 11(b), this WT spectrum is observed over *four* decades of energy, and *three* decades of spatial scales. This result⁴ constitutes the clearest and most striking numerical observation of weak turbulence spectra to date. Alternatively, when $\Gamma_1 \gg \Gamma_2$ (stronger dissipation on large spatial scales), the state relaxes to the *inverse* WT cascade, as clearly shown in Fig. 11(c). We emphasize that throughout these studies of freely decaying turbulence, the states, although decaying, decrease very slowly in the L^2 norm, and remain nonlinear throughout the time course of the numerical experiments.

For focusing nonlinearity, in addition to the two WT spectra, there is a *third* spectrum emerging under relaxation dynamics [see Fig. 11a]—a thermodynamic equilibrium of equipartition of energy: $n(k) \sim \omega(k)^{-1} \sim k^{-1/2}$. Unlike the defocusing case, focusing nonlinearity can destabilize long waves when their amplitude is sufficiently large, and create (through the modulational instability) spatially localized coherent structures, whose statistical behavior can be captured by a “most probable state description,” which predicts that these states live in thermodynamic equilibrium. Similar scenarios have been observed in the case of perturbed NLS equations.³¹ In the context of nondissipative NLS equations, a recent equilibrium statistical theory for most probable states successfully predicts coherent structures and energy equipartition.^{39,40}

We now turn to a *fourth* spectrum (MMT), which is shown in Fig. 12 for the defocusing nonlinearity. This steady state is achieved by random forcing (Gaussian white noise in time) on low k , with strong damping at high $|k| > K_d$. Our numerical experiments demonstrate that, with defocusing nonlinearity, a state with MMT spectrum can be very long lived. Moreover, in some

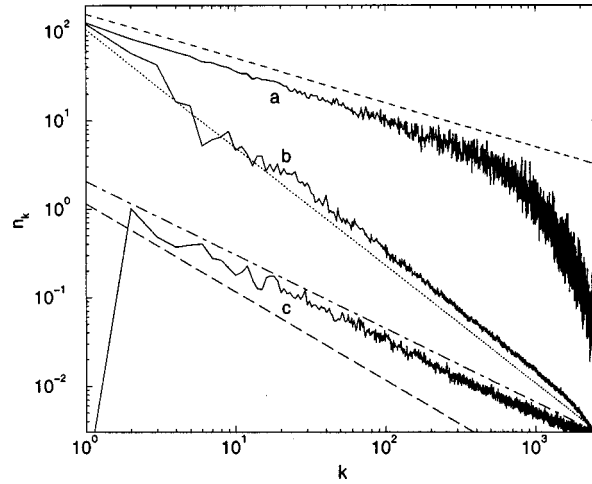


FIG. 11. (a) *Thermodynamical equilibrium* under relaxation dynamics (focusing nonlinearity, $\alpha = \frac{1}{2}$, $\sigma = 0.25$). The short dashed line has the slope of energy equipartition, $n(k) \sim \omega(k)^{-1}$. (b) *Direct cascade* WT spectrum under relaxation dynamics (defocusing nonlinearity, $\alpha = \frac{1}{2}$, $\sigma = -0.125$). The slope of the dotted line is the prediction of the WT theory for the direct cascade. (c) *Inverse cascade* WT spectrum under relaxation dynamics (defocusing nonlinearity, $\alpha = \frac{1}{2}$, $\sigma = 0$). The slope of the dot-dashed line is the prediction of WT theory for the inverse cascade. For comparison, the prediction of the WT direct cascade is also shown (dashed line). Note that, for clarity, spectra (b) and (c) have been shifted down by a factor of 10 and 100, respectively.

focusing cases, the MMT spectrum can persist for a very long time—as long as $\sim 3 \times 10^5$ time units (not shown). The MMT spectra reported in Ref. 37 were in this weakly nonlinear regime.

Finally, we present a case of the *defocusing* nonlinearity, in which (numerically) the MMT spectrum describes statistical steady states. Figure 13 shows an example in which the defocusing dynamics initially exhibits a WT direct cascade, but eventually becomes the MMT spectrum. This transition from the WT direct cascade to the MMT spectrum provides our strongest numerical evidence that the MMT can describe a stable statistically steady state. (Alternatively, for much weaker damping in the high k dissipative range, we note that a WT direct cascade describes the statistical steady state.)

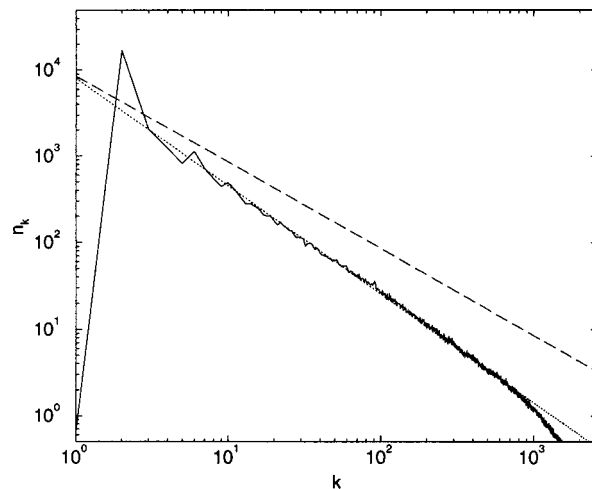


FIG. 12. *MMT spectrum* of driven-damped dynamics (defocusing nonlinearity with $\alpha = \frac{1}{2}$, $\sigma = 0$). The system is driven by a random force at $|k| = 2$ and is damped at $|k| = 1$ and $|k| > 2600$. The slope of the dotted line is the prediction of the MMT closure and, for comparison, the dashed line has the direct WT cascade slope.

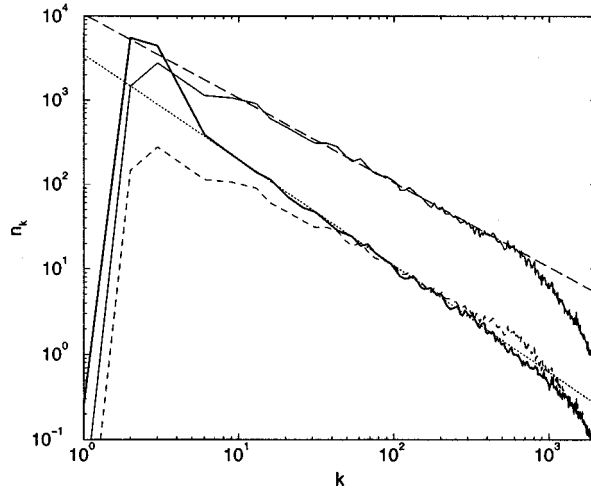


FIG. 13. MMT (thick line) state as the statistically steady state in the *defocusing* dynamics ($\alpha = \frac{1}{2}$, $\sigma = 0$), driven by a random force, which evolves from a transient WT direct cascade. The WT direct cascade is indicated by the short dashed line and, for clarity, is shifted up by a factor of 10, as indicated by the fine line. The dotted line has the MMT exponent and the dashed line has the WT direct cascade exponent.

Having established the existence of four distinct stable spectra, we next examine more detailed behavior such as distinctions between the focusing and defocusing cases, and the role of localized coherent structures in dispersive wave turbulence.

B. Deterministic forcing

With steady (time-independent) forcing, the system is completely deterministic and any turbulence that is observed is a form of spatiotemporal chaos in a deterministic system. In this setting we observe clear distinctions between focusing and defocusing nonlinearities.

When the system is driven by steady (time-independent) forcing on low $|k|$'s, the *defocusing* dynamics has a spectrum shown in Fig. 14(a), which exhibits a statistically steady state with the coexistence of a direct WT spectrum on high k 's and a resonance spectrum on low k 's. These Hamiltonian resonances permeate from low k through intermediate k 's and create a "stochastic layer" on higher k 's. Waves in this stochastic layer in turn pump energy to high k 's and induce sufficient decoherence of those high k waves to result in a WT direct cascade. In contrast, for *focusing* nonlinearity with steady driving at a moderate amplitude, the motion of long waves becomes chaotic due to modulational instability, which quickly generates a wave turbulence inertial range starting from very low k 's. In this focusing case, initially the MMT spectrum is observed over the entire initial range. However, it is a transient and the WT direct cascade spectrum gradually invades from low k 's, while the range of the MMT spectrum shrinks toward high k 's and eventually disappears, leaving the WT spectrum over the entire inertial range. Figure 14(b) shows an intermediate stage of this transition, in which both spectra coexist.

Distinctions between the focusing and defocusing nonlinearities are also apparent in the space-time profiles of the turbulent waves. As shown in Fig. 15, coherent structures that are very localized in space dominate the spatial profile in the focusing case, in contrast with the defocusing case, where the turbulent waves ride on the long-wavelength "global" radiation modes, which are driven by the low- k deterministic force (Fig. 16).

If we trace the phase, $\phi(x,t) = \text{Arg } q(x,t)$, of the wave $q(x,t)$, the dynamics of focusing nonlinearity exhibits far more chaotic phase evolution than that of defocusing nonlinearity, as shown in Figs. 17 and 18. Plotted is the function $\phi(x,t)$ evenly sampled in time. Figure 18 shows that, for the defocusing case, the phase of the wave is more or less "locked" (at $\phi \sim \pi$ in the

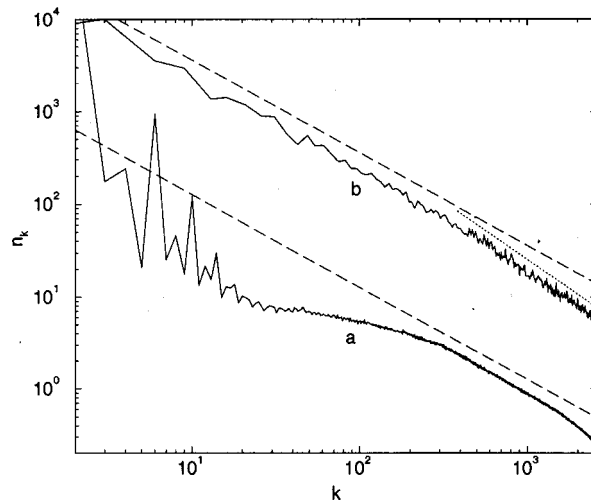


FIG. 14. *Steady deterministic force.* (a) Coexistence of a WT direct cascade with Hamiltonian resonances in a statistically steady state, for the *defocusing* dynamics ($\alpha = \frac{1}{2}$, $\sigma = 0$), driven by a steady force on $2 \leq |k| \leq 4$. (b) Invasion of a WT direct cascade into the MMT transient regime, for the *focusing* nonlinearity ($\alpha = \frac{1}{2}$, $\sigma = 0$), driven by a steady force on $2 \leq |k| \leq 3$. The initial data for these cases is smooth, composed of a simple sum of $A_i \operatorname{sech}(A_i(x - x_i))$, $1 \leq i \leq 3$, the location x_i being arbitrarily chosen. Note that spectrum (b) has been shifted up by a factor of 10^2 for clarity.

figure) to the external forcing, with a small random spattering around the locking phase. (Note that π and $-\pi$ should be identified). In contrast, Fig. 17 displays an efficient randomization of the phase over the entire interval $[-\pi, \pi]$ for the focusing nonlinearity.

The efficiency of chaoticization as illustrated in the phase of the wave has strong implications for the validity of weak turbulence. Recall that the essence of weak-turbulence theories is that the distribution of turbulent waves are nearly Gaussian, which leads to mean-field closures for kinetic equations. Strong phase randomization as in the focusing case naturally indicates Gaussian random phase approximation, and, thus, indicates the validity of a weak-turbulence description of wave turbulence. Our numerical study confirms this argument: Gaussianity is well satisfied for the focusing nonlinearity, as shown in Fig. 19 for all a_k —this underlies the observation of the weak-turbulence direct cascade over the entire inertial range in Fig. 14(b). Note that for a Gaussian distribution of a complex variable, the n th moment, m_n , is related to m_2 by $m_n = c_n m_2^{p_n}$, where $c_4 = 2$, $p_4 = 2$, $c_6 = 6$, and $p_6 = 3$. In the focusing case, our numerical values for the exponents agree with these theoretical values within 2% and those for the $c_{4,6}$ within 5%—indicating a high

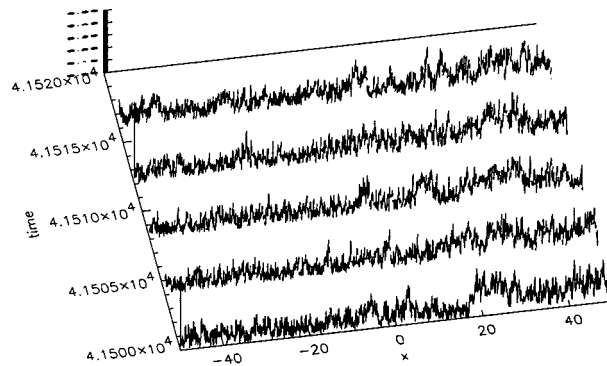


FIG. 15. *Focusing nonlinearity:* Localized coherent structures in the evolution of system (30) under a time-independent deterministic forcing on $2 \leq |k| \leq 3$ and a constant damping Γ_2 for $k > K_d$, $\alpha = \frac{1}{2}$, $\sigma = 0$. Plotted here is $|q(x,t)|$. Only a small portion of the total system $L = 410$ is shown.

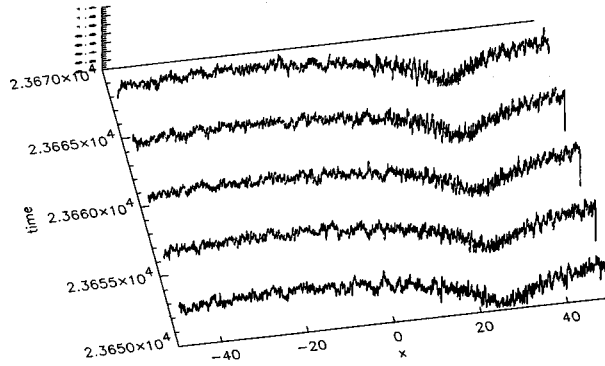


FIG. 16. Defocusing nonlinearity: Turbulent waves riding on coherent long-wavelength modes in the evolution of system (30) under a time-independent deterministic forcing on $2 \leq |k| \leq 4$ and a constant damping Γ_2 for $k > K_d$, $\alpha = \frac{1}{2}$, $\sigma = 0$. Plotted here is $|q(x,t)|$. Only a small portion of the total system $L = 410$ is shown.

degree of Gaussianity since the deviation from $c_{4,6}$ is a more stringent test for Gaussianity. In contrast, for the case of the defocusing nonlinearity under a deterministic forcing, as shown in Fig. 20, there is more than 10% deviation from p_6 and nearly 100% deviation from c_6 , indicating a large deviation from Gaussianity. As expected, this non-Gaussianity gives rise to a non-WT resonance spectrum over a large k range in Fig. 14(a). Interestingly, Fig. 20 shows that only for small $n(k)$ is there a roughly approximate Gaussian region, which precisely corresponds to the region in high k 's in Fig. 14(a), where a weak-turbulence direct cascade is observed.

Thus, one distinction between the focusing and defocusing cases is the manner and efficiency by which the deterministic force at small k is converted into an “effective random stirring” of the intermediate spatial scales. In the focusing case, this conversion is very efficient, relies on the modulation instability, involves only relatively small k modes, with completely random phases. On the other hand, in the deterministic defocusing case, the absence of the modulational instability forces the conversion to be less efficient, and to take place through a larger range of k modes (presumably through a breakdown of KAM tori), with limited phase randomization.

We mention that, although the defocusing case in Fig. 14 has stronger nonlinearity than the focusing case in Fig. 14—e.g., the L^2 norm, N , for the defocusing case is $N \sim 27$ while $N \sim 7$ for the focusing case, the focusing nonlinearity exhibits a far larger inertial range. For the defocusing nonlinearity, a sufficient strong nonlinearity is required for a possible chaoticization of wave

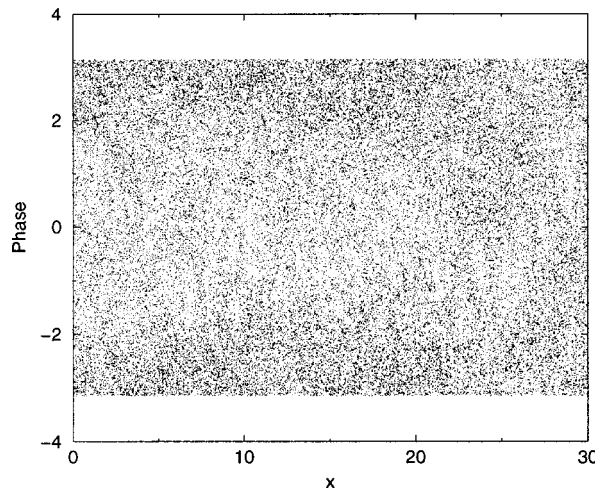


FIG. 17. Chaotic phase distribution for the focusing nonlinearity under deterministic drive.

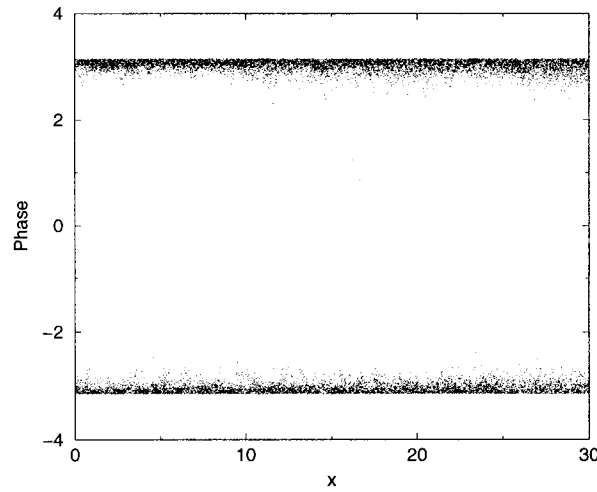


FIG. 18. Phase distribution for the *defocusing* nonlinearity under deterministic drive.

motions. Recall that, however, weak-turbulence theories are often justified on the ground of weak nonlinearity. This obviously raises the question of how to identify a validity regime of weak turbulence for the defocusing nonlinearity under deterministic forcing.

C. The cycles of dispersive wave turbulence

The next numerical experiment illustrates, for the focusing case, the cycle of energy transfer in the statistical steady state of dispersive wave turbulence—a cycle that involves the interaction of coherent structures and resonant waves as they form the equilibrium, inverse and direct WT cascades simultaneously. As described above, modulation instability in focusing dynamics induces spatially coherent “solitonic” excitations at random spatial locations to form a thermal equilibrium bath (Fig. 21). The formation of these excitations can actively transfer energy into high k_s via their focusing processes in space, where the order of magnitude of wave number k_s is determined by the spatial scale at which these localized waves saturate. This energy injection process associated with the creation of the localized excitations is a relatively fast process, while the decay of

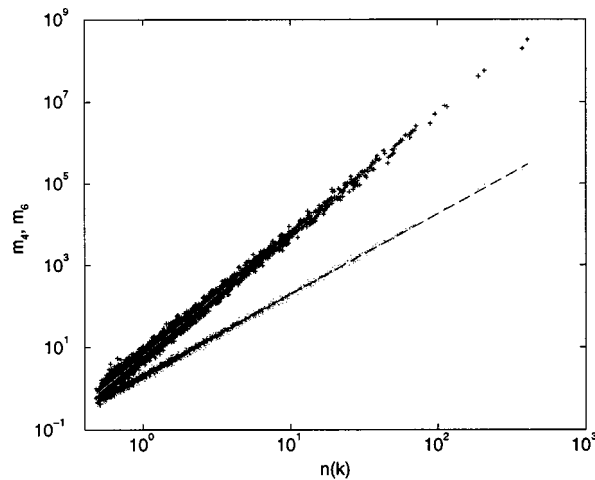


FIG. 19. Gaussianity for the *focusing* nonlinearity under a deterministic drive. The best fit for the sixth moment (crosses) as a function of the second moment is $m_6 = 6.30 m_2^{2.95}$ (white line) and for the fourth moment (dots) is $m_4 = 2.05 m_2^{1.98}$ (dashed line). Note that $m_2 = n(k)$ and the relations $m_6 = 6 m_2^3$ and $m_4 = 2 m_2^2$ hold for Gaussian distribution.

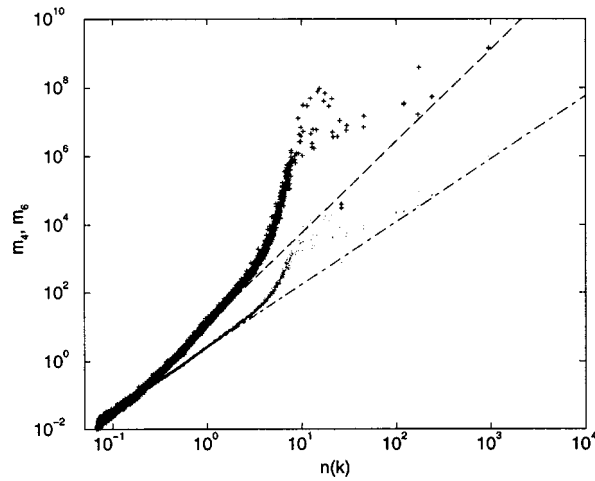


FIG. 20. Deviation from Gaussianity for the *defocusing* nonlinearity under deterministic drive. The best fit (dashed line) for the nearly power law tail for the sixth moment (crosses) as a function of the second moment is $m_6 = 11.9 m_2^{2.62}$ and the best fit (dot-dashed line) for the fourth moment (dots) is $m_4 = 2.54 m_2^{1.84}$. Note that $m_2 = n(k)$ and the relations $m_6 = 6 m_2^3$ and $m_4 = 2 m_2^2$ hold for Gaussian distributions.

these coherent structures is slow. At moderate forcing amplitudes, the saturation process occurs at intermediate spatial scales, and k_s resides in the middle of the inertial range; however, at large forcing amplitudes, the saturation process occurs at very short wavelengths, and k_s resides within the dissipation range. In the latter case, some radiation is dissipated and some generates, through resonant quartet interactions, an inverse cascade toward long wavelengths—where the modulational instability acts to create self-focusing coherent structures and complete the cycle. In the former case (of moderate forcing amplitudes), the saturating states in the center of the inertial

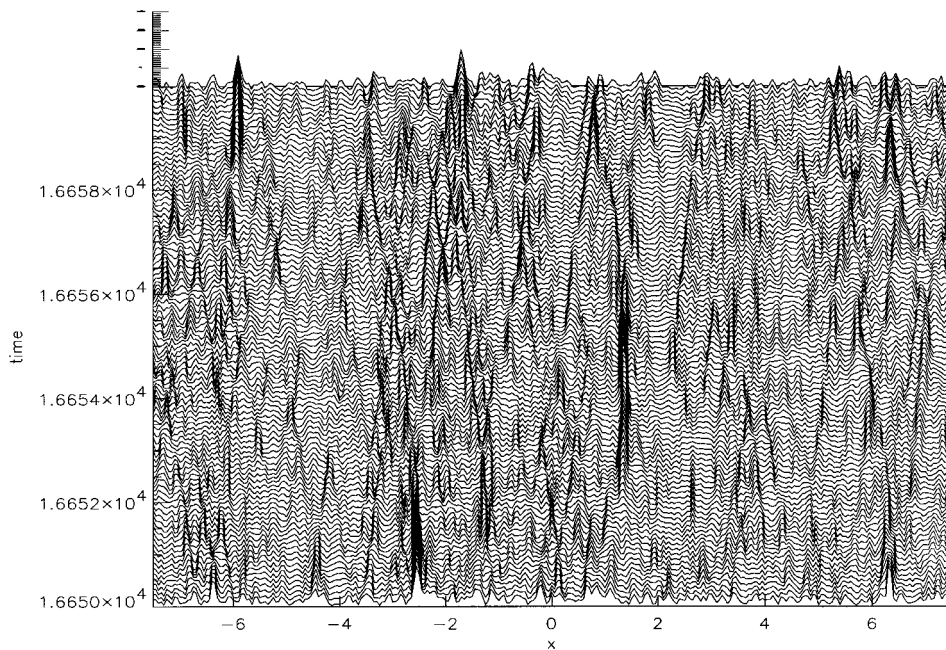


FIG. 21. Formation of the coherent structures, their saturation, and the generation of the inverse cascades (which can be observed in the decay process of those localized structures into long-wavelength radiation). Plotted here is the space-time profile of $|q(x,t)|$. ($\alpha = \frac{1}{2}$, $\sigma = 0$, focusing nonlinearity).

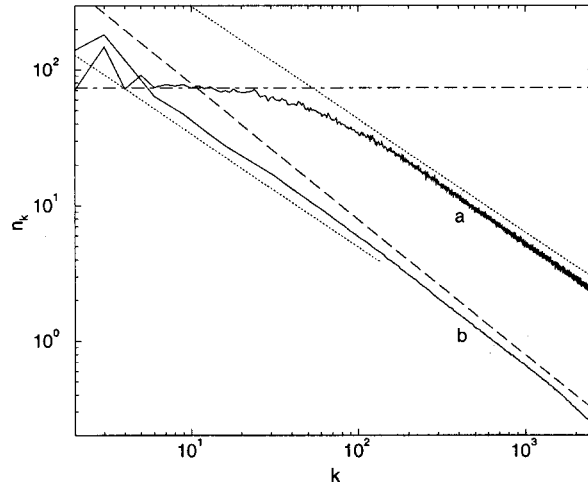


FIG. 22. (a) Coexistence of thermodynamical equilibrium and the *inverse* WT cascade, for the *focusing* nonlinearity ($\alpha = \frac{1}{2}$, $\sigma=0$), driven by a steady force on $|k|=1$. The flat part of the spectrum (dot-dashed line) shows thermodynamical equilibrium. (b) Coexistence of the *inverse* and *direct* WT cascades. The dotted (dashed) line has the exponent of the *inverse* (direct) WT cascade.

range generate, again through resonant quartet interactions, both the direct (toward shorter scales) and the inverse (toward longer scales) cascades. Dissipation terminates the flux toward shorter scales, and the modulational instability terminates the flux (of the inverse cascade) toward longer scales. And again, the cycle continues.

Figure 22(a) shows an excellent example of the coexistence of a thermodynamical equilibrium state of these coherent structures and the inverse cascade induced by their slow radiation of long coherent waves. For spectrum (a), we have $k_s > 1000$. We note that, for k higher than k_s , the usual WT direct cascade should be expected, since the coherent excitations do not have a strong influence on energy transfer at spatial scales much smaller than their coherence length. Figure 22(b) demonstrates this phenomenon, where we have tuned the dynamics to a regime such that only very few long waves are unstable. These inject energy into $k_s \sim 100$, resulting in an inverse cascade for $k < k_s$ and a direct cascade for $k > k_s$. [To help in the interpretation of these equilibrium spectra, we note that, in general, the distribution for the thermodynamical equilibrium is $1/(\omega + \mu)$, where μ is chemical potential. We are able to specify the value of μ in our experiments by controlling the forcing strength. The thermodynamical equilibrium distribution of those unstable long modes \tilde{k} in Fig. 22 corresponds to the limit in which $\mu \gg \omega(\tilde{k})$, whereas, spectrum *a* in Fig. 11 corresponds to the case of $\mu = 0$, i.e., $n(k) \sim \omega(k)^{-1}$.]

The formation and decay of coherent excitations in thermal equilibrium, together with the resonance wave interaction of the direct and inverse cascades, form a complete cycle of energy transfer in the statistical steady state—in contrast from standard descriptions in plasma turbulence, which primarily utilize collapse with high- k dissipation.⁴¹ Notice that the location of the spatial scale k_s at which the coherent structures saturate depends upon the strength of the nonlinearity (which can be controlled by the strength of amplitude of the external forcing). This saturation wave number k_s can reside either within the inertial range or within the dissipation scales. When it resides within the inertial range, both the direct and inverse cascades are present. Figure 23 illustrates schematically the energy transfer cycle in these two situations. In a freely decaying situation, the cycle changes dynamically. As the turbulence decays, the saturation scale k_s moves from the high- k dissipation scale of strong nonlinearity, through the intermediate inertial range where both cascades appear, to the low- k injection range itself, where only a weak turbulence direct cascade remains. Finally we point out that, even when driven extremely strongly, e.g., a value so strong that the total norm is increased by a factor of 10^2 with respect to the cases shown

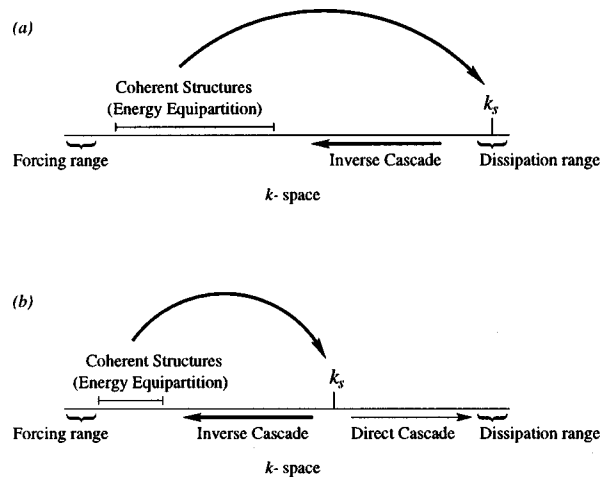


FIG. 23. The cycle of energy transfer in dispersive wave turbulence. (a) The saturation scale k_s of the spatially localized coherent structures is in the dissipation range—Coexistence of energy equipartition and the WT inverse cascade. (b) The saturation scale k_s of the spatially localized coherent structures is in the middle of the inertial range—Coexistence of the WT inverse cascade and direct cascade.

in Fig. 22, the *defocusing* dynamics does not possess this energy transfer cycle simply because it does not have long wave instabilities, and *localized* excitations.

D. Summary

As shown above, there are rich spectra of the dispersive wave turbulence within the single model (30)—the direct and inverse cascades of weak-turbulence theory, thermodynamic equilibrium, and the MMT spectrum. The weak turbulence spectra are intrinsic properties of free waves, while the MMT spectrum is associated with a damped-driven situation. It seems that the MMT spectrum usually arises in the force dominating regime, wave front propagation of focusing waves in k space,⁴ or as a steady-state matching to driving and dissipation. Although the WT cascade spectra and thermodynamic equilibrium spectra can be encapsulated by a single theoretical framework, namely, weak-turbulence theory, in order to fully understand this MMT spectrum, it seems that we need more insight into matching asymptotics between the inertial range and forcing/dissipation ranges. In other words, understanding the full dynamics of wave turbulence will require a weak-turbulence theory which takes into account fully the noninertial effects of forcing and damping. In addition to the confirmation of wave turbulence spectra, we have also demonstrated that the interplay among these wave turbulence spectra in the focusing case is controlled by spatially localized, coherent structures—in the focusing case, the instability of long waves creates spatially randomly distributed, coherent structures, which inject energy into the high- k region and establish an energy transfer cycle within wave turbulence, thus, giving rise to the coexistence of multiple turbulence spectra in a statistically steady state.

VII. CONCLUSION—EFFECTIVE STOCHASTIC DYNAMICS AND PREDICTION

States of spatiotemporal chaos exist. In the setting of *dispersive wave turbulence* these states can be comprised of spatially localized coherent structures in interaction with the fluctuating radiation waves of the “active heat bath.” These deterministic wave systems act as if they were stochastic. While a basic and fundamental description of the (universal ?) properties of the active nonlinear heat bath is important, for applications it is even more important to develop equations that predict macroscopic transport of observable quantities. In the chaotic deterministic systems of dispersive wave turbulence, one seeks effective stochastic equations with which to quantify the behavior of coherent structures and other macroscopic observables.

Fundamental issues and questions immediately arise: Which properties and observables can be predicted? Do properties exist for which prediction is impossible in principle? Is it possible to describe these deterministic systems of spatiotemporal chaos by an effective stochastic dynamics? Can an effective stochastic dynamics be realized in principle and in practice? If so, how can the equations of effective stochastic dynamics be constructed and verified? Such issues are just beginning to be addressed in the literature.

The first fundamental issue is the existence and realizability of an effective stochastic dynamics. This issue was initially studied by Zalesky³³ in the setting of spatiotemporal chaos for the Kuramoto–Sivashinsky nonlinear wave equation. Earlier, Yakhot³⁴ had proposed, using very heuristic renormalization arguments, that the longest waves in this deterministic spatiotemporal chaotic system could be described by a stochastically forced Burgers' equation with a renormalized diffusion coefficient. Zalesky designed and performed some numerical experiments on the original deterministic Kuramoto–Sivashinsky equation, which provided positive evidence that such an effective stochastic dynamics could indeed exist. Later, in the setting of a damped-driven NLS equation, we^{31,32} refined these numerical studies, making them more detailed and precise. Our work confirmed Zalesky's original conclusions; moreover, it established that the existence of an effective stochastic dynamics demands only temporal chaos and does not require spatiotemporal chaos. Furthermore, our numerical results are consistent with the notion that spatiotemporal chaos with increasing large domains (or the number of modes) can give rise to Gaussianity of the effective stochastic forcing—in this limit, thus, a universal description of effective stochastic force may be available for macroscopic dynamics.

Very recently, in their mathematical study of idealized models for stochastic climate prediction, Majda, Timofeyev, and Vanden Eijnden⁴² developed an effective stochastic dynamics for a single climate variable U , and tested its predictions against the original Hamiltonian system (with 57 degrees of freedom). Here the effective stochastic dynamics provided successful prediction in the presence of the "active heat bath."

Effective stochastic dynamics appears indeed to be realizable. However, procedures for the construction of stochastic dynamics for the original system are not well understood and need to be further developed. Fundamental issues of predictability emerging out of these developments await to be addressed and clarified. Such topics will be active areas of research for the next decade.

ACKNOWLEDGMENTS

David Cai is supported in part by the Joseph and Herbert Keller Instructorship at New York University, and in part by a Sloan Foundation Grant No. 96-3-1. David McLaughlin is supported in part by a Sloan Foundation Grant No. 96-3-1, AFOSR-49620-98, and NSF DMS-9971813.

¹M. Cross and P. Hohenberg, "Pattern formation outside of equilibrium," *Rev. Mod. Phys.* **65**, 851–1112 (1993).

²D. W. McLaughlin and E. A. Overman, "Whiskered tori for integrable pdes and chaotic behavior in near integrable pdes," *Surveys Appl. Math.* **1**, 83–203 (1995).

³D. Cai, D. W. McLaughlin, and K. T. R. McLaughlin, "The nonlinear Schrödinger equation as both a pde and a dynamical system," *Handbook in Dynamical Systems* (to appear).

⁴D. Cai, A. J. Majda, D. W. McLaughlin, and E. G. Tabak, "Spectral bifurcations in dispersive wave turbulence," *Proc. Natl. Acad. Sci. USA* **96**, 14 216–14 221 (1999).

⁵C. S. Gardner, J. M. Greene, M. D. Kruskal, and R. M. Miura, "Method for solving the KdV equation," *Phys. Rev. Lett.* **19**, 1095–1097 (1967).

⁶P. D. Lax, "Integrals of nonlinear equations of evolution and solitary waves," *Commun. Pure Appl. Math.* **21**, 467–490 (1968).

⁷V. E. Zakharov and A. B. Shabat, "Exact theory of two-dimensional self-focusing and one-dimensional self-modulation of waves in nonlinear media," *Sov. Phys. JETP* **34**, 62–69 (1972).

⁸T. B. Benjamin and J. F. Feir, "The disintegration of wave trains on deep water," *J. Fluid Mech.* **27**, 417–430 (1967).

⁹V. E. Zakharov, Ph.D. thesis, 1966.

¹⁰N. Ercolani, M. Forest, and D. McLaughlin, "Geometry of the modulational instability, III: Homoclinic orbits for the periodic sine Gordon equation," *Physica D* **43**, 348–384 (1990).

¹¹Y. Li and D. W. McLaughlin, "Morse and Melnikov functions for NLS pdes," *Commun. Math. Phys.* **162**, 175–214 (1994).

¹²V. I. Arnold, "Instabilities of systems with several degrees of freedom," *Sov. Math. Dokl.* **5**, 581–585 (1964).

- ¹³N. M. Ercolani and D. W. McLaughlin, "Toward a topological classification of integrable PDE's," *The Geometry of Hamiltonian Systems* (Springer-Verlag, New York, 1991).
- ¹⁴A. R. Bishop, M. G. Forest, D. W. McLaughlin, and E. A. Overman, II, "A quasiperiodic route to chaos in a near-integrable pde," *Physica D* **23**, 293–328 (1986).
- ¹⁵J. Guckenheimer and P. Holmes, *Nonlinear oscillations, dynamical systems, and bifurcations of vector fields* (Springer-Verlag, New York, 1983).
- ¹⁶S. Wiggins, *Global Bifurcations and Chaos: Analytical Methods* (Springer-Verlag, New York, 1988).
- ¹⁷Y. Li, D. W. McLaughlin, J. Shatah, and S. Wiggins, "Persistent homoclinic orbits for a perturbed nonlinear Schrödinger equation," *Commun. Pure Appl. Math.* **49**, 1175–1255 (1996).
- ¹⁸D. W. McLaughlin and J. Shatah, "Melnikov analysis for PDE's," in *Dynamical Systems and Probabilistic Methods in Partial Differential Equations*, Berkeley, CA, 1994 (American Mathematical Society, Providence, RI, 1996), pp. 51–100.
- ¹⁹S. Smale, "Differential dynamical systems," *Bull. Am. Math. Soc.* **73**, 747–817 (1967).
- ²⁰Y. Li, "Smale horseshoes and symbol dynamics in perturbed NLS equations," *J. Nonlinear Sci.* **9**, 363–415 (1998).
- ²¹C. Zeng, "Homoclinic orbits for perturbed NLS equation," to appear in *Comm. Pure Appl. Math.*
- ²²G. Haller, "Homoclinic jumping in the perturbed nonlinear Schrödinger equation," *Commun. Pure Appl. Math.* **52**, 1–47 (1999).
- ²³G. Haller, *Chaos Near Resonance* (Springer-Verlag, New York, 1999).
- ²⁴G. Cruz Pacheco, C. D. Levermore, and B. Luce, "Melnikov methods for Pde's with applications to perturbed nonlinear Schrödinger equation," *Physica D*, to appear. 2000.
- ²⁵M. G. Forest, C. G. Goedde, and A. Sinha, "Chaotic transport and integrable instabilities in a near-integrable, many-particle, Hamiltonian lattice," *Physica D* **67**, 347–386 (1993).
- ²⁶M. J. Ablowitz and B. M. Herbst, "Numerically induced chaos in the nonlinear Schrödinger equation," *Phys. Rev. Lett.* **62**, 2065–2068 (1989).
- ²⁷M. J. Ablowitz, B. M. Herbst, and C. M. Schober, "The nonlinear Schrödinger equation: asymmetric perturbations, traveling waves and chaotic structures," *Math. Comput. Simul.* **43**, 3–12 (1997).
- ²⁸A. Calini, N. Ercolani, D. W. McLaughlin, and C. M. Schober, "Melnikov analysis of numerically induced chaos in the nonlinear Schrödinger equation," *Physica D* **80**, 227–260 (1996).
- ²⁹M. J. Ablowitz, J. Hammack, D. Henderson, and C. Schober, in preparation.
- ³⁰R. E. Blahut, *Principles and Practice of Information Theory* (Addison-Wesley, New York, 1988).
- ³¹D. Cai, D. McLaughlin, and J. Shatah, "Spatiotemporal chaos and effective stochastic dynamics for a near integrable nonlinear system," *Phys. Lett. A* **253**, 280–286 (1999).
- ³²D. Cai, D. McLaughlin, and J. Shatah, "Spatial temporal chaos for perturbed NLS equations," in preparation.
- ³³S. Zaleski, "A stochastic model for the large scale dynamics of some fluctuating interfaces," *Physica D* **34**, 427–438 (1989).
- ³⁴V. Yakhot, "Large scale properties of unstable systems governed by the Kuramoto Sivashinski equation," *Phys. Rev. A* **24**, 642–644 (1981).
- ³⁵K. Sneppen, J. Krug, M. H. Jensen, C. Jayaprakash, and T. Bohr, "Dynamic scaling and crossover analysis for the Kuramoto–Sivashinsky equation," *Phys. Rev. A* **46**, R7351–7354 (1992).
- ³⁶G. Goren, J. Eckmann, and I. Procaccia, "Scenario for the onset of space–time chaos," *Phys. Rev. E* **57**, 4106–4134 (1998).
- ³⁷A. J. Majda, D. W. McLaughlin, and E. G. Tabak, "A one dimensional model for dispersive wave turbulence," *J. Nonlinear Sci.* **7**, 9–44 (1997).
- ³⁸V. E. Zakharov, "Kolmogorov spectra in weak turbulence problems," in *Basic Plasma Physics II* (North-Holland, New York, 1984), pp. 1–36.
- ³⁹R. Jordan, B. Turkington, and C. Zirbel, "A mean field statistical theory for the NLS equation," *Physica D* **137**, 353–378 (2000).
- ⁴⁰R. Jordan and C. Josserand, "Self organization in nonlinear wave turbulence," *Phys. Rev. E* **61**, 1527–1539 (2000).
- ⁴¹A. C. Newell and V. E. Zakharov, "Optical turbulence," in *Turbulence: A Tentative Dictionary*, edited by P. Tabeling and O. Cardoso (Plenum, New York, 1995), pp. 59–66.
- ⁴²A. Majda, I. Timofeyev, and E. Vanden Eijnden, "Models for stochastic climate prediction," *Proc. Natl. Acad. Sci. USA* **96**, 14 687–14 691 (1999).